Available online at www.sciencedirect.com
SCIENCE DIRECT®
Journal of Sound and Vibration 281 (2005) 675–697
JOURNAL OF SOUND AND VIBRATION
www.elsevier.com/locate/jsvi

Buffeting response of long-span cable-supported bridges under skew winds. Part 2: case study

Y.L. Xu[a], L.D. Zhu[b,*]

[a]*Department of Civil and Structural Engineering, The Hong Kong Polytechnic University, Hung Hom, Kowloon, Hong Kong, China*
[b]*State Key Laboratory for Disaster Reduction in Civil Engineering, Department of Bridge Engineering, Tongji University, 1239 Siping Road, Shanghai 200092, China*

Received 4 April 2003; received in revised form 20 October 2003; accepted 20 January 2004
Available online 18 September 2004

Abstract

The finite-element-based framework for buffeting analysis of long-span cable-supported bridges under skew winds has been presented in Part 1 of this paper. The framework is now applied to the Tsing Ma Suspension Bridge in Hong Kong as a case study. The wind velocities and bridge responses measured by the Wind and Structural Health Monitoring System (WASHMS) of the bridge during Typhoon Sam in 1999 are first analyzed to find the skew wind characteristics surrounding the bridge, the modal damping ratios and acceleration responses of the bridge. The buffeting responses of the bridge under skew winds during Typhoon Sam are then computed using the wind characteristics and modal damping ratios measured from the field and the aerodynamic coefficients and flutter derivatives of the bridge deck and tower measured from the wind tunnel under skew winds. The computed acceleration responses of the bridge deck and cable are finally compared with the responses measured from the field. The comparison is found to be satisfactory in general and the case study forms a good practical demonstration for the verification of the proposed method for buffeting analysis of long-span cable-supported bridges under skew winds.

*Corresponding author. Tel.: +86-21-65983116X2309; fax: +86-21-65984882.
E-mail address: ledong@mail.tongji.edu.cn (L.D. Zhu).

0022-460X/$ - see front matter © 2004 Elsevier Ltd. All rights reserved.
doi:10.1016/j.jsv.2004.01.025

1. Introduction

With the continuous enhancement of computer capacity and the demand for more accurate prediction of buffeting response of modern long-span cable-supported bridges, buffeting analysis methods have been developed and refined continuously as mentioned in Part 1 of this paper. On the other hand, wind and health monitoring systems have been installed on several long-span cable-supported bridges located in wind-prone areas throughout the world to ensure the safety and normal operation of the bridges. These systems provide good opportunities for examining and improving currently used buffeting analysis methods through the comparison between computed and field measured bridge responses under various wind conditions. Among them is the "Wind And Structural Health Monitoring System" (WASHMS) installed by the Highways Department of the Hong Kong Special Administrative Region (HKSAR) of China [1] on the Tsing Ma Suspension Bridge.

On 22 August 1999, Typhoon Sam hit Hong Kong at the eastern part of its territory. The wind velocities and bridge responses of the Tsing Ma suspension bridge were timely recorded by the WASHMS. These field measurement data are used in this paper for a case study to examine the finite-element (FE)-based approach, which has been presented in Part 1 of this paper, for buffeting analysis of long-span bridges under skew winds in the frequency domain. The field measurement data are processed first to obtain the relevant wind characteristics surrounding the bridge, modal damping ratios and acceleration response of the bridge. The buffeting response of the bridge under skew winds during Typhoon Sam is then computed using the proposed method and taking the wind characteristics and modal damping ratios measured from the field and the aerodynamic coefficients and flutter derivatives of the bridge deck and tower measured from the wind tunnel under skew winds [2–4] as input parameters. The computed bridge responses are finally compared with the bridge responses measured in the field to present a good practical demonstration for the verification of the proposed approach, which may be applied in near future in suspension bridge design or performance evaluation.

2. Tsing Ma Bridge and WASHMS

2.1. Tsing Ma Bridge

The Hong Kong new international airport is located at Lantau Island. The major transportation link between the new airport and the existing commercial centers of Kowloon and Hong Kong Island is the Lantau Fixed Crossing with the Tsing Ma Bridge as its key structure. The Tsing Ma Bridge, crossing over the channel between Tsing Yi Island and Ma Wan Island, is a suspension bridge with an overall length of 2160 m and a main span of 1377 m (see Fig. 1). It carries a dual three-lane highway on the upper level of the deck and two railway tracks and two carriageways on the lower level within the deck box (see Fig. 2). The box deck is of a hybrid steel structure with 41 m wide and 7.643 m high. The east Ting Yi tower and the west Ma Wan tower are of pre-stressed concrete with 206 m high each. The two main cables with diameter of 1.1 m are of 36 m apart in the north and south and are accommodated by the four saddles located at the top of the bridge towers. On the Tsing Yi side, the main cables are extended from

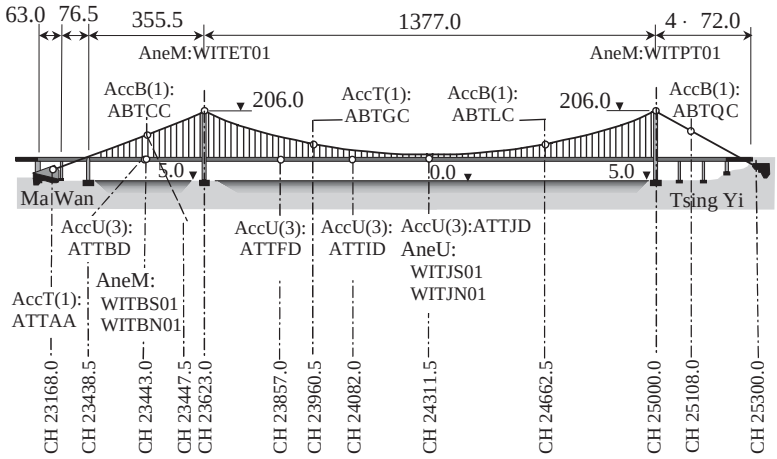

Fig. 1. Bridge elevation and sensor arrangement.

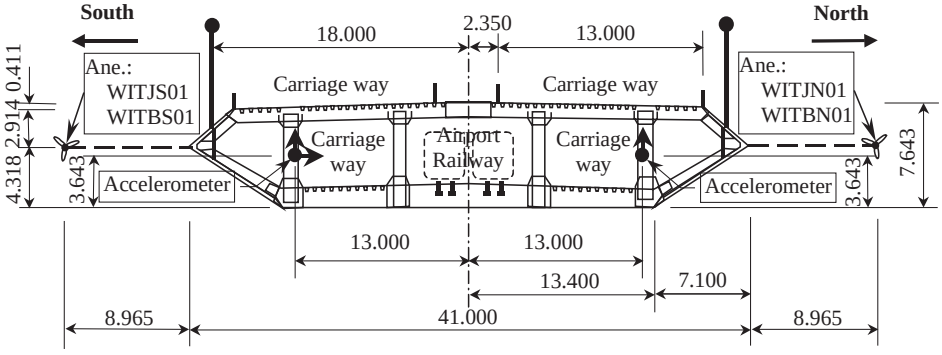

Fig. 2. Deck cross-section and sensor positions.

the tower saddles to the main anchorage through the splay saddles, forming the 300 m Tsing Yi side span. On the Ma Wan side, the main cables extended from the Ma Wan tower are held first by the saddles on the pier at a horizontal distance of 355.5 m from the Ma Wan tower and then by the main anchorage through splay saddles at the Ma Wan abutment. The alignment of bridge deck deviates for 17° in anti-clockwise from the east–west axis.

2.2. *Wind and structural health monitoring system (WASHMS)*

To monitor the structural health status of the Tsing Ma Bridge, a "Wind And Structural Health Monitoring System" (WASHMS) was installed on the bridge by the Highways Department of HKSAR [1]. There were seven different types of sensor in the WASHMS, including 6 anemometers and 24 uni-axial servo-type accelerometers. Two digital Gill Wind Master Ultrasonic Anemometers (AneU) were installed on the north side and south side, respectively,

of the bridge deck at the mid-main span. They are specified as WITJN01 and WITJS01 in Figs. 1 and 2. Each ultrasonic anemometer could measure three components of wind velocity simultaneously. Two analogue mechanical anemometers (AneM) were located at two sides of the bridge deck near the middle of the Ma Wan side span, specified as WITBN01 at the north side and WITBS01 at the south side (see Figs. 1 and 2). Each analogue mechanical anemometer consisted of a horizontal component (RM YOUNG 05106 horizontal anemometer) and a vertical component (RM YOUNG 27106 vertical anemometer). Another two analogue mechanical anemometers (AneM) of horizontal component only were arranged above the top of each bridge tower (217.084 m in elevation). They are specified as WITPT01 for the Tsing Yi tower and WITET01 for the Ma Wan tower (see Fig. 1). The sampling frequencies of all anemometers were set at 2.56 Hz and the cut-off frequency was 1.28 Hz.

The servo-type accelerometers were of the brand Allied Signal Aerospace Q-Flex QA700. Three different types of arrangement for acceleration measurement were used in the system. As shown in Fig. 1, AccT represents tri-axial measurement with three uni-axial accelerometers assembled orthogonally to each other. AccB indicates bi-axial measurement with two uni-axial accelerometers assembled perpendicularly to each other. AccU means uni-axial measurement with only one accelerometer to give signal in one prescribed direction. A total of 12 uni-axial accelerometers were used in AccU measurement and located at the four sections of the bridge deck. At each section, there were two accelerometers, horizontally separated by 13 m, measuring acceleration in the vertical direction and one accelerometer measuring acceleration in the lateral direction (see Fig. 2). The sampling frequencies of all accelerometers were set at 25.6 Hz and the cut-off frequency was 12.8 Hz.

3. Field measurement results

3.1. Typhoon Sam

On 19 August 1999, the tropical depression Sam developed at about 680 km north-east of Manila and intensified into a tropical storm sweeping across the northern part of Luzon on the next day. After moving north-westerly for almost 2 days, Typhoon Sam made landfall over the eastern part of Hong Kong near Sai Kung at about 18:00 of Hong Kong Time (HKT) on 22 August 1999. Typhoon Sam then weakened gradually over inland Guangdong on 23 August (see Fig. 3). The Hong Kong Observatory recorded a maximum hourly-mean wind speed of 27 m/s and a maximum gust wind speed of 41 m/s at 75 m high at Waglan Island during the passage of Typhoon Sam. The lowest instantaneous pressure at mean sea level was recorded as 979.0 hPa [5].

3.2. Wind characteristics

After a careful examination of all wind data recorded during Typhoon Sam, 1 h record of wind data between 14:11 to 15:11 HKT on 22 August 1999 was selected for this case study. Within this hour, incident wind blew to the bridge from the north–northeast. The wind data recorded by the anemometers at the south side of the bridge deck were thus contaminated due to the bridge deck itself, and they were not suitable for the analysis of natural wind structures.

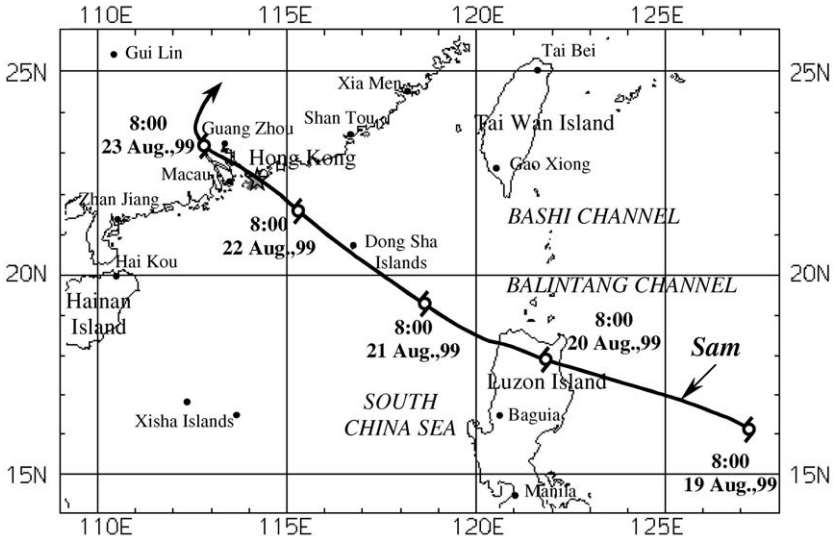

Fig. 3. Moving track of Typhoon Sam.

Furthermore, the mechanical anemometers installed on the bridge were out of order during Typhoon Sam. As a result, only the wind data recorded by the ultrasonic anemometer WITJN01 at the mid-span of the bridge were analyzed to obtain wind characteristics surrounding the bridge.

Within this specified hour, the hourly-mean wind speed $\bar{U}$ was found to be 17.1 m/s and the global hourly-mean wind yaw angle β_0 and inclination θ_0 were, respectively, -29.15° and 2.25°, according to the definitions given in Part 1 of this paper. The turbulence intensities were about 18.6%, 20.4% and 14.5%, in the longitudinal, lateral, and vertical direction, respectively, at the bridge deck level. The corresponding integral scales of turbulence were 228, 116, and 84 m, respectively, estimated according to the Taylor's hypothesis [6] and the nonlinear least-squares fitting technique. The friction velocity u^* was calculated as 1.69 m/s from the estimated horizontal shear stress τ_H using the following equations [7]:

$$u_* = \sqrt{\tau_H/\rho}; \tau_H = \rho\sqrt{(\overline{uw})^2 + (\overline{vw})^2}, \tag{1}$$

where ρ is the air density; and $u(t)$, $v(t)$, $w(t)$ are the alongwind, horizontal lateral, and upward turbulence component, respectively. In the spectral analysis, the piecewise smoothing method and the Hamming window were adopted and the nonlinear least-squares fitting technique were used to reduce the random error of spectral estimates. One-hour time history was divided into 11 sub-segments of 10 min duration each with an overlapped length of 5 min between two neighboring segments. The 1536 data points in the 10 min sub-segment were zero-padded to 2048 points to meet the requirement of fast fourier transform (FFT). The frequency resolution in the wind spectral analysis was 0.00175 Hz. Fig. 4 shows the one-side normalized auto-spectra of alongwind turbulent component $u(t)$, horizontal lateral turbulent component $v(t)$ and upward turbulent component $w(t)$. The auto-spectra were fitted using the nonlinear least-squares method with the

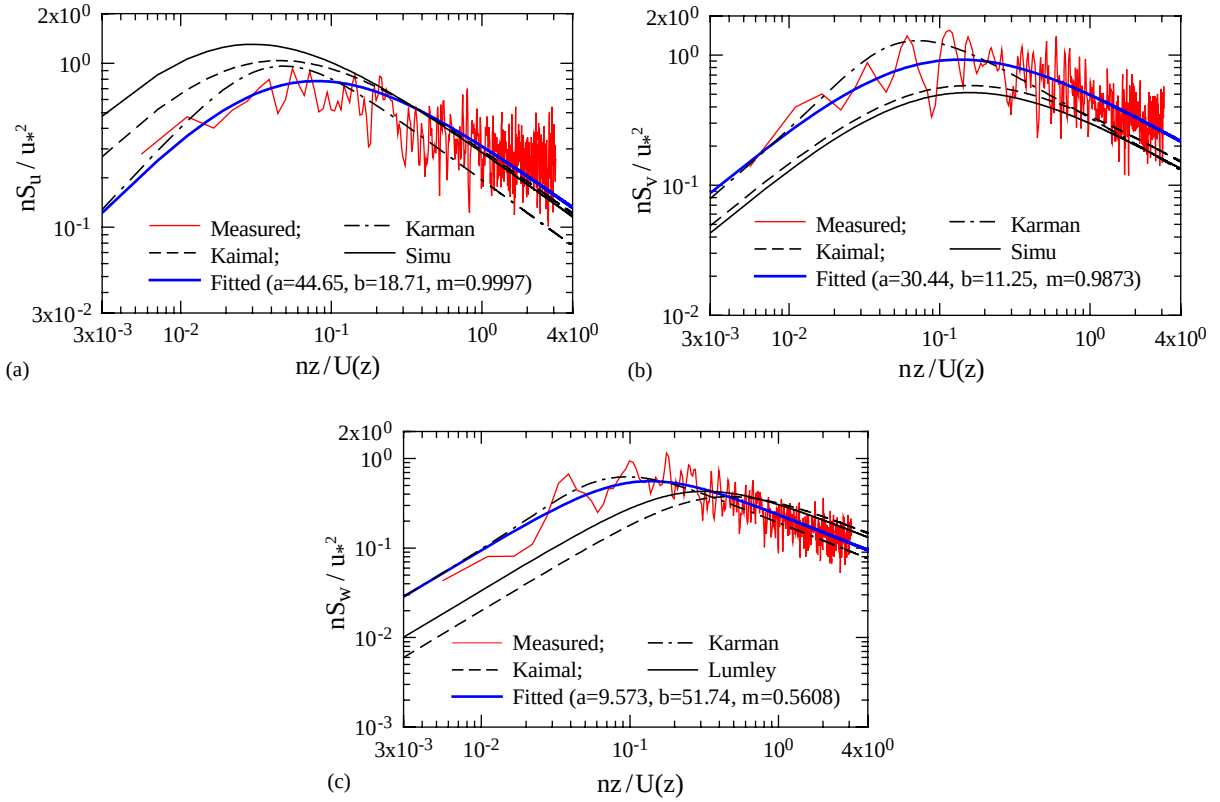

Fig. 4. Auto-spectra of fluctuating wind speeds. (a) Alongwind component $u(t)$; (b) horizontal lateral component $v(t)$; (c) upward component $w(t)$.

following target function:

$$nS_a/u_*^2 = af_z/(1 + bf_z^{1/m})^{cm} \tag{2}$$

$$f_z = nz/\bar{U}(z), \tag{3}$$

where the subscript a can be any one of u, v, w_j, n is the frequency of wind turbulence in Hz, the value of c was set to $\frac{5}{3}$, z is the height of the bridge deck about the sea level, and a, b, and m are the three parameters to be fitted. The fitted parameters and curves together with the von Karman spectra [8], the Kaimal spectra [9], the Simiu spectra [6], and the Lumley spectrum [10] are also plotted in Fig. 5. It is seen that the spectra expressed by Eq. (2) can fit the measured spectral data well in both low- and high-frequency regions. The von Karman spectra, using measured integral scales and intensities of turbulence, fit the measured spectra better than the Kaimal and Simiu spectra, especially in the low-frequency region.

The co-spectra and quadrature spectra between every two of the three fluctuating wind components were also analyzed in the form of two-side spectrum and are plotted in Figs. 5 and 6, respectively. The curve fitting using nonlinear least-squares technique was carried out for these cross-spectra by taking Eq. (2) with $c = 2.4$ as the target function. It can be seen from these spectra

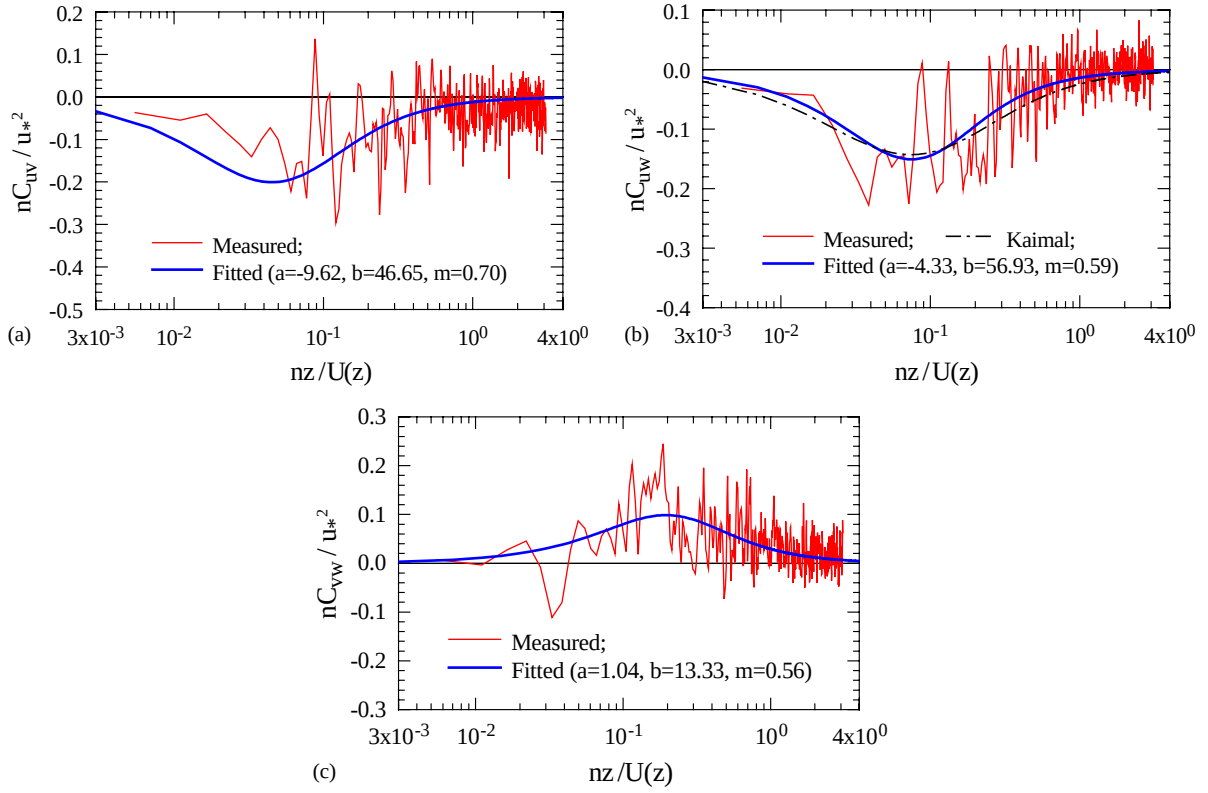

Fig. 5. Co-spectra of fluctuating wind speeds. (a) Between u and v; (b) between u and w; (c) between v and w.

that the selected target function is quite suitable for the co-spectra, but it seems not so good for the quadrature spectra. Furthermore, it is interesting to see from Fig. 5 that the spectrum using the empirical expression suggested by Kaimal et al. [9] is quite close to the fitted spectrum.

3.3. *Responses of acceleration*

Acceleration responses of the Tsing Ma Bridge during Typhoon Sam were also recorded by the WASHMS at the four deck sections and four cable sections as shown in Fig. 1. To be consistent with wind analysis, only the data recorded from 14:11 to 15:11 HKT on 22 August 1999 were analyzed and presented. The lateral acceleration response of the bridge deck directly came from the lateral accelerometer. The vertical acceleration response of the bridge deck was obtained by averaging the accelerations recorded by the two vertical accelerometers. The torsional acceleration response was calculated from the difference of the two vertical accelerations divided by 26m, the horizontal distance between the two vertical accelerometers (see Fig. 2).

3.3.1. *Root mean square (rms) responses*

In this paper, the rms responses of the measured accelerations are calculated directly from the measured acceleration history by statistical approach, whilst the computed rms responses

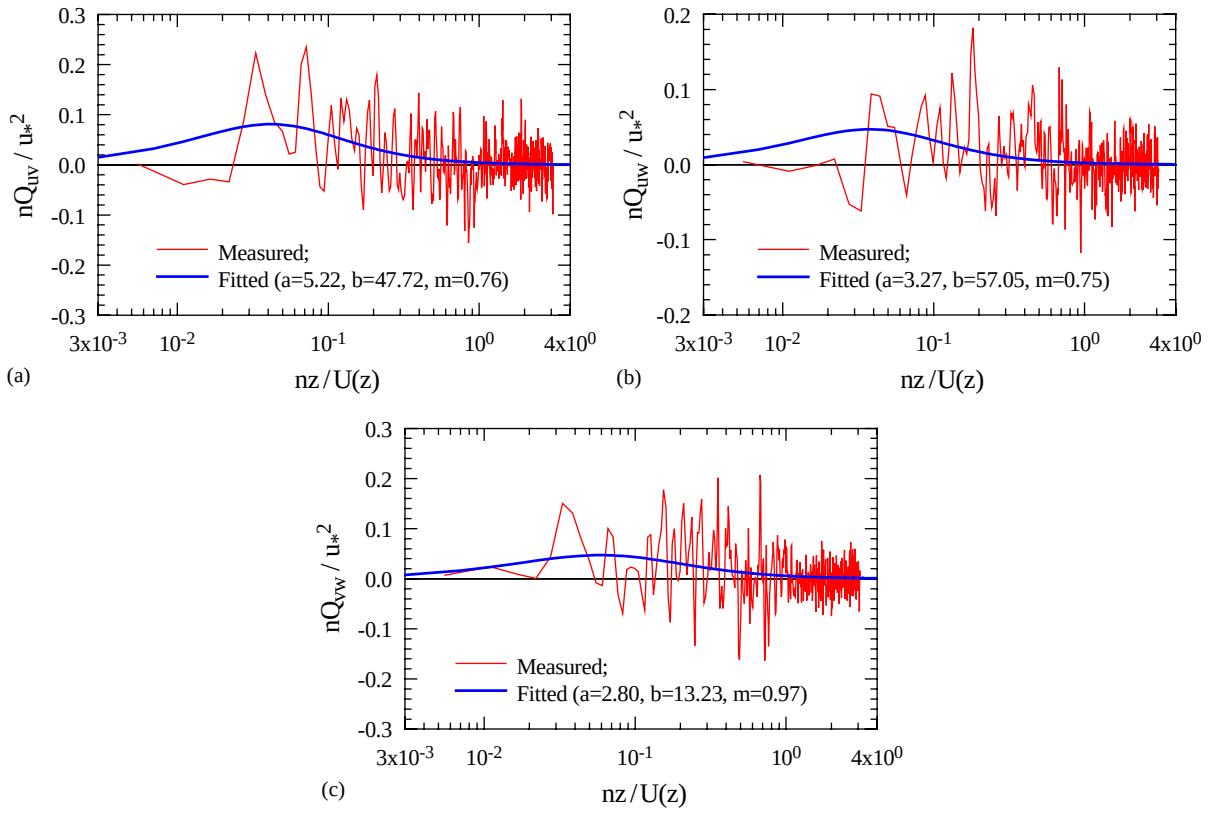

Fig. 6. Quadrature spectra of fluctuating wind speeds. (a) Between u and v; (b) between u and w; (c) between v and w.

are obtained by integrating the corresponding computed response spectra within an adequate range of frequency. Since the flutter derivatives of the Tsing Ma Bridge deck measured under skew winds are available only for the reduced velocity $\bar{U}/fB$ lower than 18 [4], namely, only for the frequency higher than 0.0232 Hz when the mean wind speed $\bar{U}$ is 17.1 m/s and the deck width (B) is 41 m, the same lower- and upper-frequency bounds of the integrating range are set as 0.025 Hz and 0.75 Hz, in which 0.75 Hz is higher than the 45th natural frequency (0.7062 Hz) of the bridge. Therefore, to have a reasonable comparison between computed and measured buffeting responses, the measured acceleration signals should go through a digital bandpass filter with the same lower- and upper-frequency bounds of frequency as used in the computation. The rms acceleration responses of the bridge deck and cable calculated from the measured response time histories with the bandpass filter are listed in Table 1. The maximum rms responses of the bridge deck are 0.012, 0.073 m/s^2 and 0.0022 rad/s^2, respectively, in the lateral, vertical and torsional directions, occurring all at the mid-main span (ATTJD) of the bridge. The responses of the bridge cable are larger than those of the bridge deck. The lateral and vertical rms responses of the bridge cable at the quarter span are 0.024 and 0.079 m/s^2, respectively.

Table 1
rms acceleration responses

Section	Deck				Cable			
	ATTJD	ATTID	ATTFD	ATTBD	ABTQC	ABTLC	ATTGC	ABTCC
Lateral (m/s^2)	0.012	0.012	0.009	0.008	0.019	0.022	0.024	0.014
Vertical (m/s^2)	0.073	0.070	0.069	0.055	0.016	0.079	0.077	0.056
Torsional*13 m (m/s^2)	0.029	0.029	0.025	0.010	—	—	—	—
Longitudinal (m/s^2)	—	—	—	—	—	—	0.019	—

Table 2
Natural frequencies and modal damping ratios in vertical vibration

No.	Frequency (Hz)				Damping ratio (%)	Dominant motion
	Computed	Ambient test	Measured	Deviation (%)		
2	0.1166	0.113	0.116	−0.5(2.7)	2.2	Deck and cables in main span
3	0.1367	0.139	0.141	3.1(1.4)	1.1	Deck and cables in main span
5	0.1890	0.184	0.184	−2.6(0.0)	1.0	Deck and cables in main span
10	0.2448	0.241	0.241	−1.6(0.0)	0.94	Deck and cables in main span
13	0.2945	0.284	0.281	−4.6(−1.1)	1.0*	Deck and cables in MW span
15	0.3246	0.327	0.328	1.0(0.3)	1.0*	Deck and cables in main span
24	0.4060	—	0.406	0.0	1.0*	Deck and cables in main span
25	0.4334	—	—	—	0.10*	Cable in TY span
27	0.4358	—	—	—	0.10*	Cables in TY span
28	0.4431	—	—	—	0.50*	Deck in longitudinal
33	0.4991	—	0.497	−0.4	1.0*	Deck and cables in main span
39	0.5989	—	0.591	−1.3	1.0*	Deck and cables in main span
41	0.6481	—	0.644	−0.6	1.0*	Deck and cables in MW span
45	0.7062	—	0.719	1.8	1.0*	Deck and cables in main span

Note: 1. The relative deviation figures out of parentheses are between the frequencies computed and measured in this field measurement whilst those in parentheses is between the frequencies measured in the ambient test and in this field measurement;
2. Modal damping ratios with '*' are estimated based on the other vibration modes of similar nature.

3.3.2. *Spectral analysis*

The acceleration response spectra were obtained by means of FFT technique on the acceleration time histories recorded at the four deck sections and the four cable sections. The number of data points for the FFT and the overlapped length were selected as 8192 and 2.6 min, respectively. As a result, 1 h data were divided into 21 segments, which were then averaged and smoothed. Meanwhile, the Hamming window was also applied, and thus the actual frequency resolution of the obtained response spectra was 0.004375 Hz.

The natural frequencies of the bridge during Typhoon Sam were then obtained from the measured response spectra. They are listed in Tables 2–4, respectively, for the lateral, vertical and torsional modes of vibration together with those computed by using the FE model of the bridge

Table 3
Natural frequencies and modal damping ratios in lateral vibration

No.	Frequency (Hz)				Damping ratio (%)	Dominant motion
	Computed	Ambient test	Measured	Deviation (%)		
1	0.0681	0.069	0.069	1.3(0.0)	1.0	Deck and cables in main span
4	0.1578	0.164	0.159	0.8(−3.0)	1.1	Deck and cables in main span
6	0.2104	0.214	0.225	6.9(5.0)	0.21	Cables in main span
7	0.2305	0.226	0.237	2.8(4.9)	0.20*	Cables in main span
8	0.2324	0.236	0.244˜ 0.247	5.0–6.3 (3.4–4.7)	0.68	Cables in main span
9	0.2401	0.240	0.244˜ 0.247	1.6–2.9 (1.7–2.9)	0.83	Cables in main span
12	0.2851	0.297	0.287	0.7(−3.4)	1.0*	Deck and cables in main span, coupled with deck torsion in main span
16	0.3331	0.336	0.350	5.1(4.2)	1.0*	Cables in MW span
17	0.3404	0.352	0.362	6.3(2.8)	0.20*	Cables in main span
18	0.3651	0.381	0.387	6.0(1.6)	0.40	Cables and deck in main span
19	0.3671	—	0.363	−1.1	0.089	Cables in MW span
20	0.3800	—	0.397	4.5	0.14	Cables in TY span
21	0.3933	—	0.419	6.5	0.094	Cables in TY span
22	0.3960	—	0.412	4.0	0.20*	Cables in main span
23	0.4040	—	—	—	0.20*	Cables in main span
26	0.4344	—	—	—	1.0*	Cables of entire bridge
30	0.4832	—	0.491	1.6	0.20*	Cables in main span
31	0.4892	—	0.488	−0.2	1.0*	Deck in main & MW spans
32	0.4964	—	0.512	3.1	0.20*	Cables in main span
34	0.5260	—	—	—	0.20*	Towers and cables
36	0.5461	—	0.550	0.7	0.18	Towers and cables
37	0.5798	—	0.591	1.9	0.20*	Cables in main span
38	0.5943	—	0.572	−3.8	0.25	Cables in main span
42	0.6686	—	0.681	1.9	1.0*	Cables in main span
43	0.6698	—	—	—	0.20*	Cables in main span
44	0.6954	—	0.700	0.7	1.0*	Deck and cables of entire bridge

Note: 1. The relative deviation figures out of parentheses are between the frequencies computed and measured in this field measurement whilst those in parentheses is between the frequencies measured in the ambient test and in this field measurement;
2. Modal damping ratios with '*' are estimated based on the other vibration modes of similar nature.

established by Xu et al. [11] and the major natural frequencies measured in an earlier ambient vibration test carried out by Xu et al. [11] on the bridge. The natural frequency number in the three tables is assigned according to the sequence of computed vibration modes of the entire bridge. The natural frequencies measured in this field measurement cover most of the first 45 computed natural frequencies but some of the computed natural frequencies could not be identified from the measured response spectra.

Table 4
Natural frequencies and modal damping ratios in torsional vibration

No.	Frequency (Hz)				Damping ratio (%)	Dominant motion
	Computed	Ambient test	Measured	Deviation (%)		
11	0.2713	0.267	0.266	−2.0(−0.4)	0.44	Deck and cables in main span, coupled with lateral bending of main span deck
14	0.3106	0.320	0.322	3.7(−0.1)	0.48	Deck and cables in main span
29	0.4755	—	0.484	1.8	0.50*	Deck and cables in main span
35	0.5392	—	0.597	10.7	0.54	Deck and cables in MW span
40	0.6162	—	0.634	2.9	0.49	Deck and cables in main span

Note: 1. The relative deviation figures out of parentheses are between the frequencies computed and measured in this field measurement whilst those in parentheses is between the frequencies measured in the ambient test and in this field measurement;
2. Modal damping ratios with '*' are estimated based on the other vibration modes of similar nature.

It is seen from Table 2 that the 13th and 41st natural frequencies correspond to the vertical motion of the Ma Wan side span. The other measured natural frequencies are associated with the vertical motion of the main span of the bridge. The difference between the three sets of natural frequencies is insignificant. The computed results show that the 25th and 27th natural frequencies are related to the vertical motion of the free cables in the Tsing Yi side span, and the 28th natural frequency is associated with the deck longitudinal motion. These three natural frequencies could not be identified from the measured acceleration spectra of the bridge deck and cable.

From Table 3 it is seen that the differences between the three sets of natural frequencies in the lateral direction are less than 7.0%. For the modes of vibration (Nos. 1, 4, 12, 31 and 44) dominated by the lateral motion of bridge deck in the main span, the differences are less than 3.5%. The good agreement among the three sets of natural frequencies provides a good foundation for the comparison of bridge buffeting response. It is seen that the lowest computed natural frequency of the bridge is 0.068 Hz, corresponding to the first lateral mode. Both the measured response spectra and the computed modes of vibration reveal that the lateral mode of the bridge deck at 0.2875 Hz (No. 12) is coupled with the deck torsional motion (see Fig. 9a and c). Furthermore, four modes of vibration (Nos. 23, 26, 34 and 43) could not be identified from the measured acceleration spectra. According to the computed mode shapes, it can be inferred that the main reason is that the accelerometers were installed close to the stationary points of the vibration modes.

As listed in Table 4, there are a total of five torsional modes identified from the measured acceleration spectra with the cut-off frequency of 0.75 Hz. Among these five torsional modes, the 35th mode of vibration reflects the torsional motion of the deck in the Ma Wan side span. All the other torsional modes represent the torsional motion of the bridge deck in the main span. Both the measured response spectra and the computed mode shapes indicate that the first torsional

vibration mode of 0.2656 Hz is coupled with the deck lateral motion. It is seen again that the difference between the three sets of natural frequencies is insignificant for the main span torsional modes, but it is more than 10% for the side span torsional mode.

3.4. Modal damping ratios

The Hilbert–Huang transform (HHT) method [12,13] in conjunction with the random decrement technique (RDT) was used to identify the modal damping ratios from the measured acceleration response time histories. Each measured acceleration response time history was first decomposed into a series of intrinsic mode functions (IMF) by using the empirical mode decomposition (EMD) method and an intermittency check method. The RDT was then applied to the IMF which represents a specified modal response of the bridge to obtain the corresponding free modal response. The Hilbert transform (HT) method was applied to the free modal response time history to identify the total damping ratio of the associated mode of vibration. Finally, the structural modal damping ratio was obtained by deducting the corresponding aerodynamic damping ratio from the identified total damping ratio. The aerodynamic damping of the bridge was estimated based on the measured flutter derivative curves presented in Ref. [4] and the measured aerodynamic coefficient curves presented in Ref. [3]. The aerodynamic damping of cable vibration in vertical and lateral direction was estimated based on the quasi-steady theory.

The identified modal damping ratios are presented in Tables 2–4. In general, the modal damping ratios associated with cable vibration are significantly lower than those related to deck vibration. For instance, the measured modal damping ratio is about 1% for the 1st and 4th modes of vibration dominated by the deck lateral motion. It becomes less than 0.1% for the 19th and 21st modes of vibration that are the pure cable lateral motion in the Ma Wan side span and in the Tsing Yi side span, respectively. It is also noticed that even for the modes of vibration dominated by the bridge deck motion in the vertical direction, the identified modal damping ratios are somehow different to some extent. The modal damping ratio in the 2nd mode of vibration reaches 2.2%, which is more than two times of the modal damping ratio in the 3rd, 5th, and 10th modes of vibration. Furthermore, the damping ratios in some vibration modes could not be extracted from the measured response time histories. This is because either some modes of vibration were closely spaced or the accelerometer was located close to the stationary point of vibration modes or the signal was contaminated by the measurement noise. To meet the demand in the buffeting analysis of the Tsing Ma Bridge using the proposed method, the damping ratios of these modes were then assigned based on the identified damping ratios for the other vibration modes of similar nature (see Tables 2–4).

4. Analyses and comparison of buffeting response

4.1. Rationality of comparison of buffeting response

To have a reasonable comparison of bridge buffeting response between the field measurement and computation, the wind speed used in the buffeting analysis should not be in the vicinity of the wind speed associated with either aeroelastic instability or vortex shedding. In fact, the critical

wind speed of the Tsing Ma Bridge associated with aeroelastic instability was estimated to be higher than 50.0 m/s for wind inclination between $\pm 5^{\circ}$ [14]. This critical wind speed is much higher than the wind speed of 17.1 m/s concerned in this comparison. Furthermore, it can be inferred from the information provided in Ref. [14] that the vortex-induced vibration of the Tsing Ma Bridge is insignificant when wind speed is 17.1 m/s. Thus, the mean wind speed of 17.1 m/s used in the comparison of buffeting response of the Tsing Ma Bridge during Typhoon Sam is considered appropriate.

4.2. Input parameters

The detailed information on the 3D FE model of the Tsing Ma Bridge can be found in Ref. [11]. The first 45 computed natural modes with the frequencies listed in Tables 2–4 were included in the buffeting analysis of the bridge in this case study. The measured or estimated modal damping ratios as listed in Tables 2–4, and the measured wind characteristics as introduced in Section 3.2, such as mean wind speed and direction, auto-wind spectra, cross-wind spectra, and friction velocity, were used in the computation as input parameters. Because of the limitation of the measurement system, the mean wind speed and direction were considered to be uniform along the bridge deck in the computation. According to the local wind code [15], the power law with the exponent of 0.33 was adopted to describe the mean-wind profile. The exponential decay coefficients for the determination of the root-coherence functions and cross-spectra of two fluctuating wind components at two separate spatial points could not be estimated from the field measurement data and were taken as $C^{u}_{X_u} = 3.0$, $C^{v}_{X_u} = 3.0$, $C^{w}_{X_u} = 3.0$, $C^{u}_{Y_v} = 16.0$, $C^{v}_{Y_v} = 11.0$, $C^{w}_{Y_v} = 8.0$, $C^{u}_{Zw} = 10.0$, $C^{v}_{Zw} = 7.0$, $C^{w}_{z_w} = 7.0$ as suggested in the Refs. [6,16]. The corresponding phase spectra were also not available at this stage and thus they were taken as zero.

The aerodynamic coefficients of the bridge deck, tower legs, and tower transverse beams used in the buffeting analysis were measured through the wind tunnel tests under skew wind condition [2,3]. The approximate formulae were used to estimate the coefficients of drag and crosswind forces of the main cables under skew winds. The aerodynamic forces on the bridge hangers (suspenders) were neglected. To include the effects of aeroelastic forces in the buffeting analysis, the eight flutter derivatives of H^{*}_{i} and A^{*}_{i} $(i = 1, 2, 3, 4)$ of the bridge deck measured under skew wind [4] were used in the computation. The flutter derivatives of P^{*}_{1}, P^{*}_{3}, P^{*}_{5}, H^{*}_{5} and A^{*}_{5} were not available from the wind tunnel tests and hence determined based on the quasi-steady theory. The remaining five flutter derivatives were considered insignificant to the bridge buffeting response and neglected in the computation.

Furthermore, there were no measurement data available on the aerodynamic admittance functions of the Tsing Ma Bridge. The empirical formulae and other measures have to be used. For the bridge tower components including tower legs and transverse beams, the aerodynamic admittance functions were set to unity. The formula suggested by Vickery [17] for the aerodynamic admittance function of circular cylinder was adopted here for the main cables. For the bridge deck, the following formula proposed by Davenport [18]:

$$\chi(nH/\bar{U}) = \sqrt{2\left(c\frac{nH}{\bar{U}} - 1 + \mathrm{e}^{-cnH/\bar{U}}\right)} \Big/ \left(c\frac{nH}{\bar{U}}\right) \tag{4}$$

was employed for the 9 aerodynamic admittance functions associated with the drag, crosswind force, and yawing moment of the bridge deck ($\chi_{C_{\tilde{q}}u}$, $\chi_{C_{\tilde{q}}v}$, $\chi_{C_{\tilde{q}}w}$, $\chi_{D_{\tilde{p}}u}$, $\chi_{D_{\tilde{p}}v}$, $\chi_{D_{\tilde{p}}w}$, $\chi_{M_{\tilde{\phi}}u}$, $\chi_{M_{\tilde{\phi}}v}$ and $\chi_{M_{\tilde{\phi}}w}$), where H is the height of bridge deck, c is the decay coefficient of the turbulence coherence along the deck chord and was taken as 7. The other 9 admittance functions associated with the lift, pitching moment, and rolling moment were set to unity. Actually, it was found from parametric studies that the set of aerodynamic admittances used here produced a quite good computed acceleration spectra, which fit the measured spectra much better than those computed using other aerodynamic admittances, such as Sears function [19] and Irwin formula [20].

4.3. Computed acceleration response and comparison

4.3.1. Acceleration response of bridge deck

The computed acceleration spectra of the bridge deck at the four sections are shown in Figs. 7–9 together with the measured spectra obtained with the bandpass filter. From the lateral response spectra shown in Fig. 7, one can see that the computed response spectra agree with the measured ones quite well for the sections ATTJD, ATTID, and ATTFD of the main span in the frequency region below 0.2 Hz. This indicates that the Davenport's aerodynamic admittance function used for the lateral vibration of the bridge is adequate. In the high-frequency range, the computed response spectra deviate from the measured response spectra to some extent. There are many factors attributed to this moderate discrepancy. However, this moderate discrepancy may not significantly affect the rms acceleration response because the spectral amplitude in the

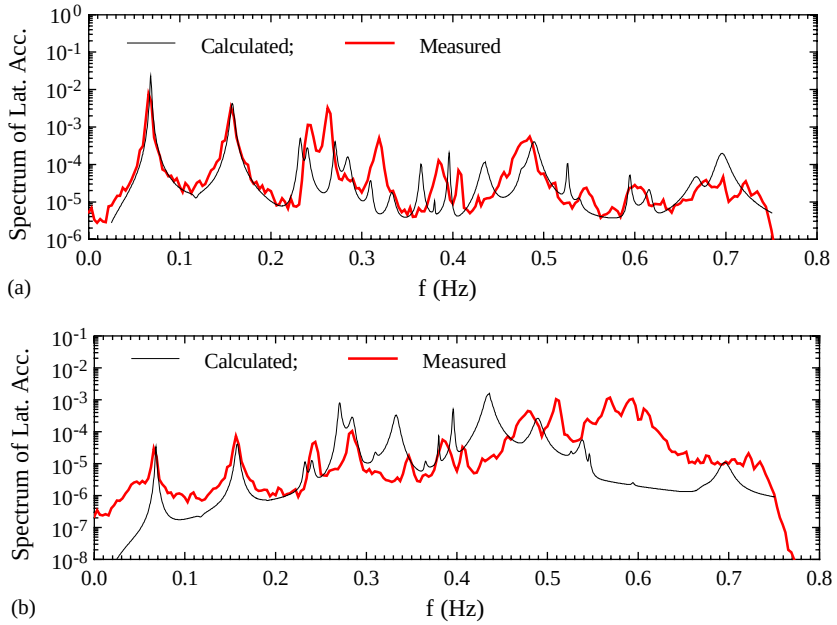

Fig. 7. Measured and computed spectra of deck lateral acceleration. (a) At section ATTID; (b) at section ATTBD.

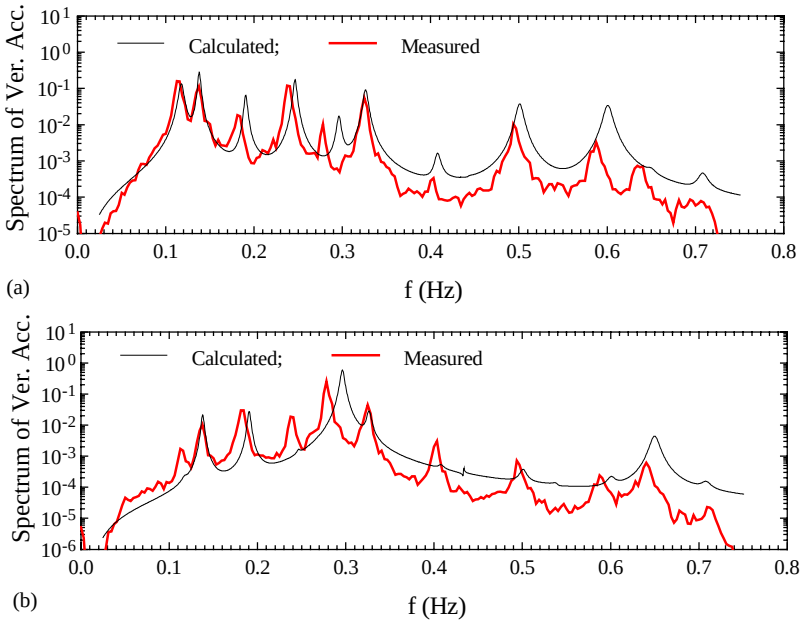

Fig. 8. Measured and computed spectra of deck vertical acceleration. (a) At section ATTID; (b) at section ATTBD.

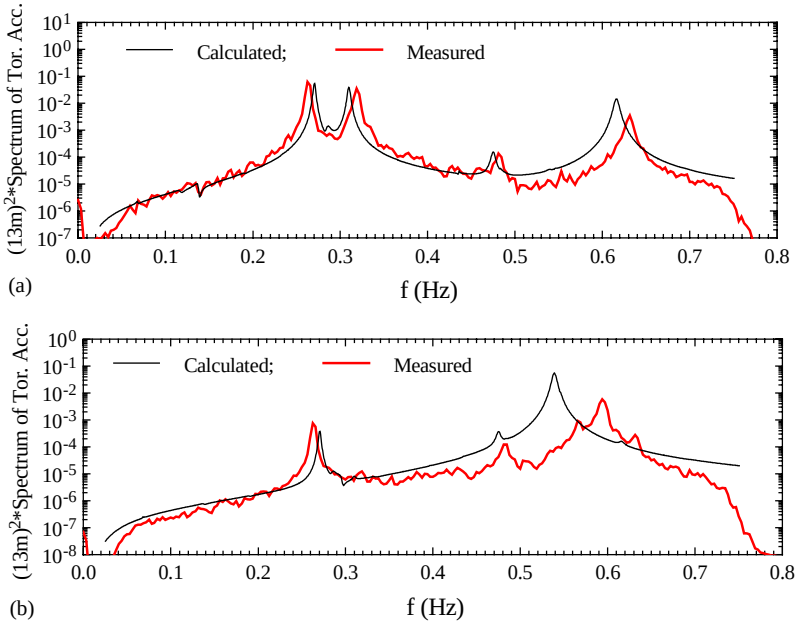

Fig. 9. Measured and computed spectra of deck torsional acceleration. (a) AT section ATTID; (b) at section ATTBD.

high-frequency range is relatively small compared with that in the low frequency range. For the deck section ATTBD in the Ma Wan side span, the dominant frequency range of large spectral amplitude is relatively high compared with the deck sections in the main span, and the discrepancy

between the computed and measured acceleration response spectra is also relatively large. For instance, the dominant peaks of the measured spectrum occur within the frequency range from 0.5 to 0.6 Hz whereas no significant peaks can be observed for the computed spectrum. On the contrary, there are three major peaks on the computed spectrum in the frequency range between 0.3 and 0.45 Hz, but the measured response spectrum is quite small within this region. Thus, one may expect that the difference between the computed and measured rms acceleration responses in the lateral direction will be large for the deck section in the Ma Wan side span.

From the vertical acceleration response spectra displayed in Fig. 8, one may find that in the frequency range lower than 0.35 Hz, the computed response spectra are in good agreement with the measured spectra for all the four bridge sections except for slight drift of some spectral peaks. In the high-frequency range, the computed spectral amplitudes are larger than the measured ones. This may be attributed to the unit aerodynamic admittance function used in the computation. The unit aerodynamic admittance may be a good approximation for the lower-frequency components but may overstate the lift force on the bridge deck in high-frequency components. One may also infer that the first vertical model damping ratio of 2.2% identified from the measured response time history is reasonable, for the computed spectra in the vicinity of the first vertical natural frequency are very close to the measured ones. On the other hand, the identified modal damping ratios (1.1%, 1.0% and 0.94%) in the second, third and fourth vertical modes of vibration may be slightly underestimated.

It is seen from Fig. 9 that the computed torsional response spectra of the three bridge deck sections in the main span are in excellent agreement with the measured torsional response spectra. The computed torsional response spectrum of the bridge deck section in the Ma Wan side span is also in good agreement with the measured one for the frequency components below 0.4 Hz. The unit aerodynamic admittance function used in the analysis for the torsional vibration of the bridge deck may be regarded satisfactory for the Tsing Ma Bridge. The torsional modal damping ratios about 0.5% identified from the measured response time history using the HHT method seems to be reasonable. The discrepancy between the computed and measured spectra of the bridge deck in Ma Wan side span comes mainly from the drift of the computed 35th natural frequency, the deviation of the aerodynamic admittance from unity in the high-frequency region, and the possible difference between the actual and used wind properties for the Ma Wan side span. In addition, the interference effect of bridge tower on the aerodynamics of the bridge deck may have some contribution to the discrepancy between the computed and measured responses of the Ma Wan side span as well.

From the computed acceleration response spectra of the bridge deck, the rms acceleration responses of the bridge deck can be obtained by the integration of the spectra in the frequency domain. The frequency range for the integration was from 0.025 to 0.75 Hz in order to have a fair comparison. The computed rms acceleration responses of the bridge deck as well as the corresponding measured ones with the bandpass filter are plotted in Fig. 10 for the lateral, vertical, and torsional vibrations, respectively. The relative discrepancies between the two sets of results are also listed in Table 5. It is seen that for the main span, the computed rms acceleration responses of the bridge deck in the lateral, vertical and torsional directions are all close to the measured results. The relative differences (RD) are less than 34% for lateral response and less than 20% for vertical and torsional response. For the Ma Wan side span, the computed rms acceleration responses in the lateral and vertical directions are also close to the measured ones.

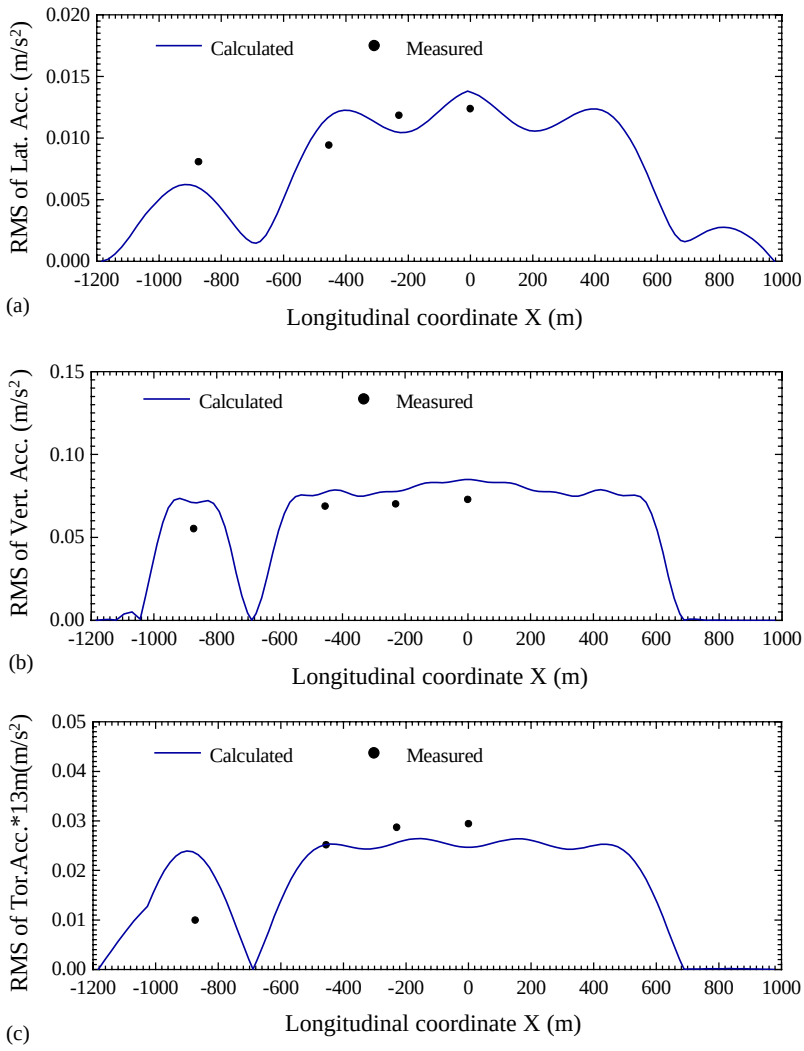

Fig. 10. Measured and computed RMS responses of deck acceleration. (a) Lateral; (b) vertical; (c) torsional.

The relative differences are less than 30%. However, for the torsional vibration, the RD between the computed and measured rms response is as high as 140%.

4.3.2. *Acceleration responses of bridge cables*

The computed and measured acceleration spectra of the main cable on the south side of the Tsing Ma Bridge are plotted in Figs. 11–13 for the lateral, vertical and longitudinal directions, respectively. From the lateral response spectra of the main cable at the four specified sections shown in Fig. 11, one may see that there is a fairly good agreement between the computed and measured spectra for the cable in the main span, but there are some moderate discrepancies in the response spectra for the cable in the two side spans. The Vickery's aerodynamic admittance used in the analysis seems to be adequate for the drag and crosswind forces on the main span cable.

Table 5
Computed deck rms acceleration responses and relative discrepancies

Section	Lateral (m/s^2)		Vertical (m/s^2)		Torsional*13 m (m/s^2)	
	Computed	RD (%)	Computed	RD (%)	Computed	RD (%)
ATTJD	0.014	16.7	0.085	16.4	0.025	−13.8
ATTID	0.010	−16.7	0.078	11.4	0.026	−10.3
ATTFD	0.012	33.3	0.077	11.6	0.025	0.0
ATTBD	0.006	−25.0	0.071	29.1	0.024	140.0

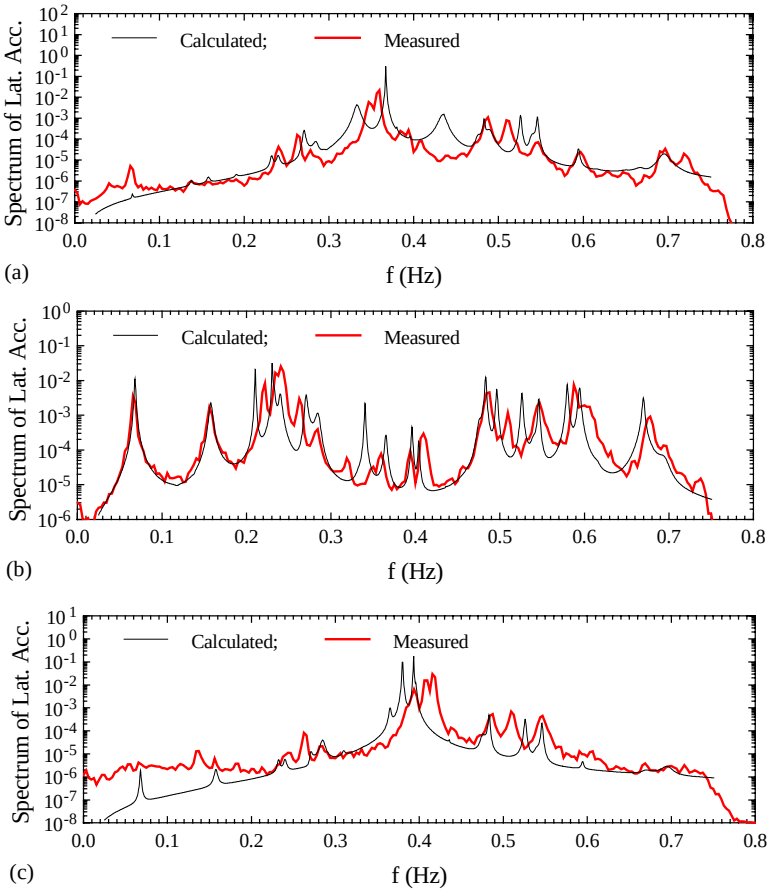

Fig. 11. Measured and computed spectra of cable lateral acceleration. (a) At section ABTCC; (b) at section ATTGC; (c) at section ABTQC.

Similar to the bridge deck, one may see from Fig. 12 that the computed vertical acceleration spectra of the main cable at the four sections agree well with the measured spectra in the frequency range below than 0.4 Hz. In the higher frequency range, the computed spectral amplitude is

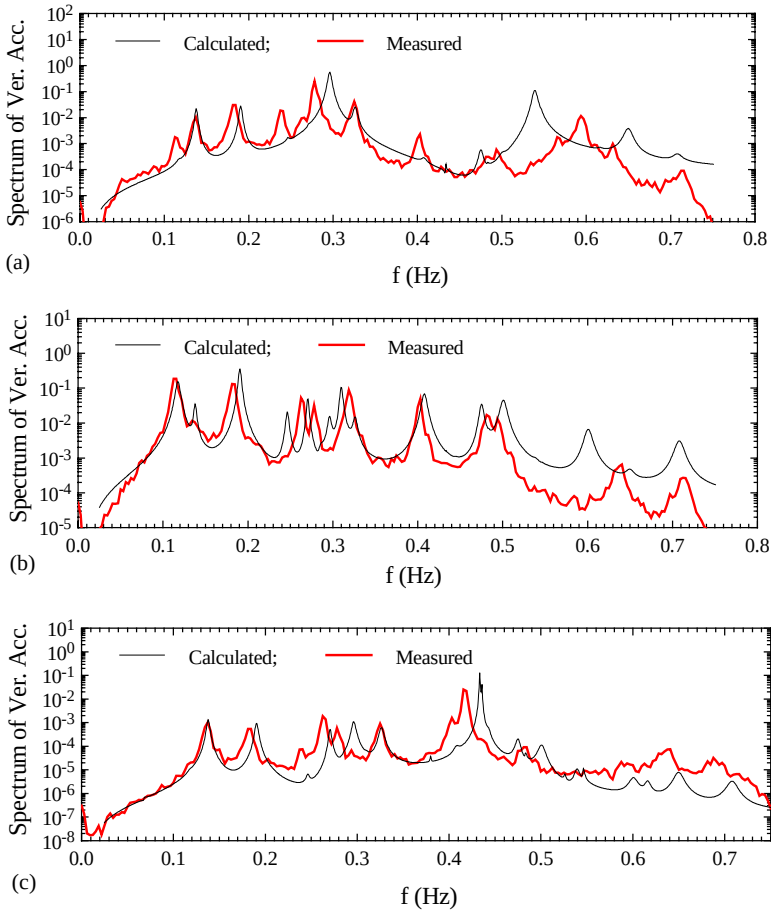

Fig. 12. Measured and computed spectra of cable vertical acceleration. (a) At section ABTCC; (b) at section ATTGC; (c) at section ABTQC.

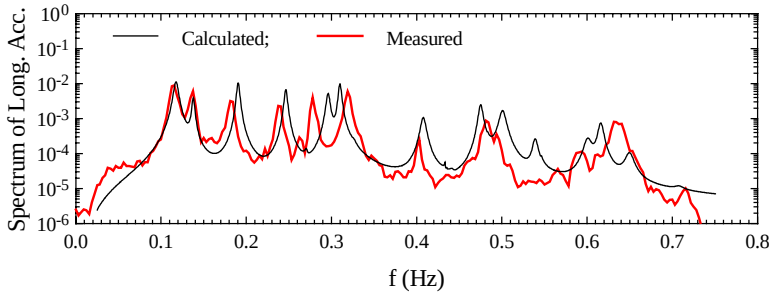

Fig. 13. Measured and computed spectra of cable longitudinal acceleration at section ATTGC.

generally higher than the measured spectral amplitude. This may be attributed to the adoption of the unit aerodynamic admittance of deck in the vertical vibration. The longitudinal acceleration response of the main cable was measured only at the section ATTGC. It is seen from Fig. 13 that

there is also a good agreement between the computed and measured response spectra of the longitudinal acceleration of the main cable.

The comparison between the computed and measured rms acceleration responses of the main cable is shown in Fig. 14 for the lateral, vertical, and longitudinal vibration, respectively. The relative discrepancies between the two sets of results are listed in Table 6. A good agreement is seen between the computed and measured rms acceleration responses for the vertical and longitudinal vibration of the cable in the main span and for the lateral and vertical vibration of the free cable in the Tsing Yi side span. The relative discrepancies are less than 11%. For the lateral acceleration of the main span cable, the computed rms acceleration responses also agree with the measured results with the discrepancies less than 21%. However, for the cable section ABTCC in the Ma Wan side span, the discrepancies between the computed and measured rms

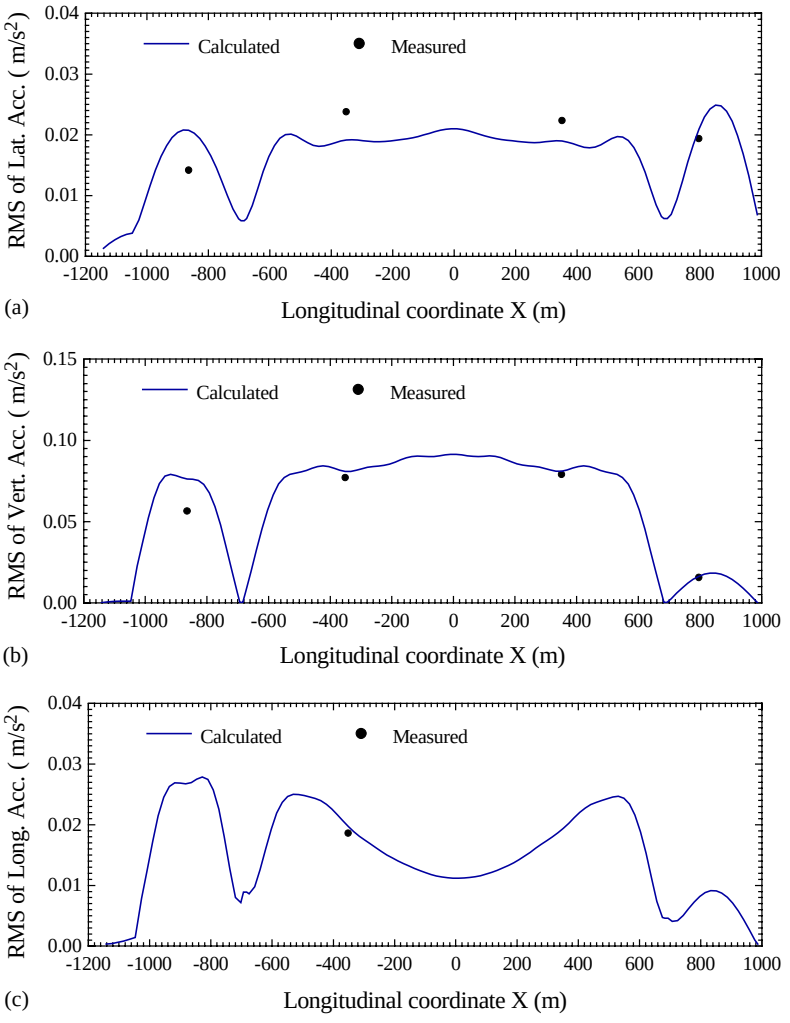

Fig. 14. Measured and computed rms responses of cable acceleration. (a) Lateral; (b) vertical; (c) longitudinal.

Table 6
Computed cable rms acceleration responses and relative discrepancies

Section	Lateral (m/s^2)		Vertical (m/s^2)		Longitudinal (m/s^2)	
	Computed	RD (%)	Computed	RD (%)	Computed	RD (%)
ABTQC	0.021	10.5	0.016	0.0	0.008	—
ABTLC	0.019	−13.6	0.081	2.5	0.019	—
ATTGC	0.019	−20.8	0.081	5.2	0.020	5.3
ABTCC	0.021	50.0	0.076	35.7	0.027	—

responses are significant for both the lateral and vertical vibrations, reaching 50.0% and 36.0%, respectively. This trend is consistent with the comparative results of the bridge deck.

5. Concluding remarks

The finite-element-based framework for buffeting analysis of long-span cable-supported bridges under skew winds, proposed in Part 1 of this paper, has been applied to the Tsing Ma suspension bridge as a case study. Wind structures and acceleration responses of the Tsing Ma Bridge measured during Typhoon Sam were analyzed. The measured wind structures of Typhoon Sam around the bridge, the aerodynamic coefficients and flutter derivatives of the Tsing Ma bridge deck and the aerodynamic coefficients of the Tsing Ma bridge tower measured from the wind tunnel under skew winds, and other relevant information were taken as input data to compute the buffeting response of the Tsing Ma Bridge. The computed buffeting responses of the Tsing Ma Bridge were then compared with the measured responses in terms of spectrum and rms value. The major comparative results are summarized as follows:

The computed response spectra agree well in general with the measured ones. The discrepancies between the computed and measured rms responses were less than 34%, 17% and 14% for the lateral, vertical and torsional vibration, respectively, of the bridge deck in the main span. The discrepancies of rms acceleration response of the main span cables were not more than 21%, 6% and 6% for the lateral, vertical and longitudinal vibration, respectively.

The considerable discrepancies between the computed and measured responses mostly occurred in the Ma Wan side span with 25%, 30%, and 140% for the bridge deck in the lateral, vertical, and torsional direction, respectively, and with 50% and 36% for the bridge cable in the lateral and vertical direction, respectively.

Nevertheless, the case study presented in this paper is just one single event or demonstration. It is obviously insufficient for the verification of the proposed method for buffeting analysis of long-span cable-supported bridges under skew winds, because some information regarding the modeling of aerodynamic forces, such as admittance functions, is not available for the Tsing Ma Bridge under skew winds and the wind characteristics measured during Typhoon Sam are not comprehensive. Therefore further investigation on these topics and more case studies with comprehensive field and wind tunnel measurements and computation of buffeting responses are needed in the future before solid conclusions can be reached. In addition, more extensive

parametric studies on, for example, wind speed effect and wind angle effects are very useful for a better understanding of the behavior of bridge response to skew winds.

Acknowledgments

The work described in this paper is financially supported by the Research Grants Council of Hong Kong (Project No. PolyU 5027/98E) and The Hong Kong Polytechnic University through the Area of Strategic Development Programme in Wind Effects on Structures, to which the writers are most grateful. The work is also a part of a research project financially supported by the National Natural Science Foundation of China (Project No. 50378068). Sincere thanks should go to Prof. H.F. Xiang of State Key Laboratory for Disaster Reduction in Civil Engineering at Tongji University, China, for his generous support and invaluable advice and Dr J. Chen of The Hong Kong Polytechnic University for his help in identifying the modal damping ratios. The writers also want to thank Mr. M.C.H. Hui for improving the English of this paper. Any opinions and concluding remarks presented in this paper are entirely those of the writers.

References

[1] C. K. Lau, K. Y. Wong, Design, construction and monitoring of the three key cable-supported bridge in Hong Kong, *Proceedings of the Fourth International Kerensky Conference on Structures in the New Millennium,* Hong Kong, 1997, pp. 105–115.

[2] L.D. Zhu, Y.L. Xu, F. Zhang, H.F. Xiang, Measurement of aerodynamic coefficients of tower components of Tsing Ma Bridge under yaw winds, *Wind and Structures* 6 (1) (2003) 53–70.

[3] L.D. Zhu, Y.L. Xu, F. Zhang, H.F. Xiang, Tsing Ma bridge deck under skew winds—part I: aerodynamic coefficients, *Journal of Wind Engineering and Industrial Aerodynamics* 90 (2002) 781–805.

[4] L.D. Zhu, Y.L. Xu, H.F. Xiang, Tsing Ma bridge deck under skew winds—part II: flutter derivatives, *Journal of Wind Engineering and Industrial Aerodynamics* 90 (2002) 807–837.

[5] Hong Kong Observatory 1999, Typhoon Sam (9910), 19–23 August 1999, http://www.info.gov.hk/hko/informtc/sam/report.htm.

[6] E. Simiu, R.H. Scanlan, *Wind Effects on Structures*, Wiley, New York, 1996.

[7] H. W. Tieleman, S. E. Mullins, The structure of moderately strong winds at a Mid-Atlantic coastal site (below 75 m), *Proceedings of Fifth International Conference on Wind Engineering*, Vol. 1, Pergamon Press, Oxford, 1980, pp. 145–159.

[8] E.E. Morfiadakis, G.L. Glinou, M.J. Koulouvari, The suitability of the von Karman spectrum for the structure of turbulence in a complex terrain wind farm, *Journal of Wind Engineering and Industrial Aerodynamics* 62 (1996) 237–257.

[9] J.C. Kaimal, J.C. Wyngaard, Y. Izumi, O.R. Cote, Spectral characteristics of surface-layer turbulence, *Journal of Royal Meteorological Society* 98 (1972) 563–589.

[10] J.L. Lumley, H.A. Panofsky, *The Structure of Atmospheric Turbulence*, Wiley, New York, 1962.

[11] Y.L. Xu, J.M. Ko, W.S. Zhang, Vibration studies of Tsing Ma suspension bridge, *Journal of Bridge Engineering, ASCE* 2 (4) (1997) 149–156.

[12] N.E. Huang, Z. Shen, S.R. Long, M.J.C. Wu, H.H. Shih, Q.N. Zheng, N.C. Yen, C.C. Tung, H.H. Liu, The empirical mode decomposition and the Hilbert Spectrum for nonlinear and non-stationary time series analysis, *Proceedings of Royal Society, London* 454 (1998) 903–995.

[13] N.E. Huang, Z. Shen, S.R. Long, A new view of nonlinear water waves: the Hilbert Spectrum, *Annual Review on Fluid Mechanics* 31 (1999) 417–457.

[14] C. K. Lau and K. Y. Wong, Aerodynamic stability of Tsing Ma bridge, *Proceedings of The Fourth International Kerensky Conference on Structures in the New Millennium*, Hong Kong, 1997, pp. 131–138.
[15] Code of practice on wind effects Hong Kong-1983, Building Development Department of Hong Kong, 1983.
[16] C. Dyrbye, S.O. Hansen, *Wind Loads on Structures*, Wiley, Chichester, England, UK, 1996.
[17] B.J. Vickery, Fluctuating lift and drag on a long cylinder of square cross-section in a smooth and in a turbulent stream, *Journal of Fluid Mechanics* 25 (3) (1966) 481–494.
[18] A.G. Davenport, Buffeting of a suspension bridge by storm winds, *Journal of the Structural Division, ASCE* 88 (ST3) (1962) 233–268.
[19] W.R. Sears, Aspects of non-stationary airfoil theory and its practical application, *Journal of the Aeronautical Sciences* 8 (1941) 104–108.
[20] H.P.A.H. Irwin, Wind tunnel and analytical investigations of the response of Lions' Gate Bridge to a turbulent wind, N.A.E. Report, LTR-LA-210, National Research Council of Canada, Ottawa, Canada, 1997.